Biosensors and Bioelectronics 175 (2021) 112875

Contents lists available at ScienceDirect

Biosensors and Bioelectronics

journal homepage: http://www.elsevier.com/locate/bios

A microdevice platform for characterizing the effect of mechanical strain magnitudes on the maturation of iPSC-Cardiomyocytes

Wenkun Dou [a,1], Li Wang [a,c,1], Manpreet Malhi [b,d,1], Haijiao Liu [a,e], Qili Zhao [a], Julia Plakhotnik [b,d], Zhensong Xu [a], Zongjie Huang [a], Craig A. Simmons [a,e,i,*], Jason T. Maynes [b,d,g,**], Yu Sun [a,e,f,h,***]

[a] Department of Mechanical and Industrial Engineering, University of Toronto, Toronto, M5S 3G8, Canada
[b] Program in Molecular Medicine, Hospital for Sick Children, Toronto, M5G 1X8, Canada
[c] School of Mechanical & Automotive Engineering, Qilu University of Technology (Shandong Academy of Sciences), Jinan, 250353, China
[d] Department of Biochemistry, University of Toronto, Toronto, M5S 1A8, Canada
[e] Institute of Biomaterials and Biomedical Engineering, University of Toronto, M5S 3G9, Canada
[f] Department of Electrical and Computer Engineering, University of Toronto, M5S 3G4, Canada
[g] Department of Anesthesia and Pain Medicine, Hospital for Sick Children, Toronto, M5G 1X8, Canada
[h] Department of Computer Science, University of Toronto, M5T 3A1, Canada
[i] Translational Biology and Engineering Program, Ted Rogers Centre for Heart Research, Toronto, M5G 1M1, Canada

ARTICLE INFO

Keywords:
Microdevice array
iPSC-CMs
Mechanical stimulation
Maturation
Contractile stress

ABSTRACT

The use of human induced pluripotent stem cell-derived cardiomyocytes (iPSC-CMs) as an *in vitro* model of the heart is limited by their structurally and functionally immature phenotypes. During heart development, mechanical stimuli from *in vivo* microenvironments are known to regulate cardiomyocyte gene expression and maturation. Accordingly, protocols for culturing iPSC-CMs have recently incorporated mechanical or electromechanical stimulation to induce cellular maturation *in vitro*; however, the response of iPSC-CMs to different mechanical strain magnitudes is unknown, and existing techniques lack the capability to dynamically measure changes to iPSC-CM contractility *in situ* as maturation progresses. We developed a microdevice platform which applies cyclical strains of varying magnitudes (5%, 10%, 15% and 20%) to a monolayer of iPSC-CMs, coincidentally measuring contractile stress during mechanical stimulation using fluorescent nanobeads embedded in the microdevice's suspended membrane. Cyclic strain was found to induce circumferential cell alignment on the actuated membranes. *In situ* contractility measurements revealed that cyclic stimulation gradually increased cardiomyocyte contractility during a 10-day culture period. The contractile stress of iPSC-CM monolayers was found to increase with a higher strain magnitude and plateaued at 15% strain. Cardiomyocyte contractility positively correlated with the elongation of sarcomeres and an increased expression of β-myosin heavy chain (MYH7) in a strain magnitude-dependent manner, illustrating how mechanical stress can be optimized for the phenotypic and proteomic maturation of the cells. iPSC-CMs with improved maturity have the potential to create a more accurate heart model *in vitro* for applications in disease modeling and therapeutic discovery.

1. Introduction

Cardiovascular diseases are a major global health burden and contribute to over 30% of deaths worldwide (Benjamin et al., 2019). The elucidation of disease pathobiology and the discovery of new treatments is limited by the difficulty of pre-clinical modeling of the heart. Human pluripotent stem cell-derived cardiomyocytes (iPSC-CMs) represent an important advancement for disease modeling, therapeutic discovery, and drug toxicity testing, providing a functionally active, renewable cell source utilizing the human proteome (Rowe and Daley, 2019). However,

* Corresponding author. Translational Biology and Engineering Program, Ted Rogers Centre for Heart Research, Toronto, M5G 1M1, Canada.
** Corresponding author. Program in Molecular Medicine, Hospital for Sick Children, Toronto, M5G 1X8, Canada.
*** Corresponding author. Department of Mechanical and Industrial Engineering, University of Toronto, Toronto, M5S 3G8, Canada.
E-mail addresses: c.simmons@utoronto.ca (C.A. Simmons), jason.maynes@sickkids.ca (J.T. Maynes), yu.sun@utoronto.ca (Y. Sun).
[1] Authors contributed equally.

https://doi.org/10.1016/j.bios.2020.112875
Received 29 September 2020; Received in revised form 9 November 2020; Accepted 28 November 2020
Available online 3 December 2020

compared with adult human cardiomyocytes, iPSC-CMs exhibit immature structural, metabolic and electrophysiological properties (Feric and Radisic, 2016). The immaturity of iPSC-CMs limits their utility as a research model, as well as their clinical application for regenerative therapy (Liu et al., 2018; Romagnuolo et al., 2019).

Within the heart, mechanical signals exerted by *in vivo* microenvironments play a critical role in (re)modelling of the myocardium, pre- and post-natally (Lindsey et al., 2014). The adaptive or maladaptive remodeling processes of human cardiomyocytes depend on local mechanical microenvironment *in vivo* (Saucerman et al., 2019). During heart development, cardiomyocytes sense mechanical stress from their microenvironment through mechanosensitive pathways, which regulate gene expression and mediate the maturation of cardiac structures and physiological functions (Feric and Radisic, 2016; Guo and Pu, 2020). Studies on cardiac development in zebrafish embryos have demonstrated the importance of mechanotransduction by showing that a lack of mechanical loading *in vivo* impedes heart development and causes abnormal formation of the heart chambers (Hove et al., 2003). Conversely, excess mechanical loading can induce maladaptive remodeling, leading to impaired heart function and cardiac diseases, such as hypertrophy and fibrosis (Saucerman et al., 2019).

Several culture techniques and tools, such as bioreactors, have incorporated mechanical stimulation to recapitulate the microenvironment of the myocardium and induce iPSC-CM maturation *in vitro* (Mihic et al., 2014; Ruan et al., 2016; Zhang et al., 2017). Either static (Ruan et al., 2016; Zhang et al., 2017) or dynamic (Banerjee et al., 2015; Mihic et al., 2014) mechanical stimulation of cardiomyocytes has promoted phenotypes consistent with a higher degree of cellular maturation, including increased cell size (Mihic et al., 2014), greater sarcomeric alignment (Zhang et al., 2017), enhanced expression of gap junction proteins (e.g. connexin-43) (Salameh et al., 2010), and upregulated transcription of genes associated with myofilaments and cardiac ion channels (Mihic et al., 2014). However, the mechanical loading conditions utilized across existing studies are inconsistent (Banerjee et al., 2015; Mihic et al., 2014; Miklas et al., 2014; Ruan et al., 2016), and the specific effects of different mechanical strain magnitudes on cardiomyocyte maturation remains unknown. Furthermore, many of these studies employed cell culturing methods which lacked the capability of effectively measuring cardiomyocyte maturation (and associated changes to contractility) *in situ*. Thus, assessment of contractility was either omitted (Feric and Radisic, 2016), or conducted as an end-point measurement by transferring tissue onto a separate platform (Ruan et al., 2016), negating the ability to optimize protocols to avoid under (lack of maturation)- or over (creating a disease phenotype)-mechanically stimulating the cells.

Here we report a microdevice array that is capable of applying dynamic mechanical stimulation on iPSC-CMs and quantitatively monitoring the evolution of cell contractility in response to different mechanical strain magnitudes *in situ*. Pneumatic pressure was applied to bulge the suspended membranes in the microdevice array for dynamic stimulation of iPSC-CMs with different strain magnitudes (0, 5%, 10%, 15% and 20%). Fluorescent nanobeads were embedded in the suspended membrane for measuring contractility of iPSC-CMs cultured on the membrane via traction force microscopy (TFM). Our results reveal that the maturation of iPSC-CMs was enhanced by mechanical stimulation in a strain magnitude-dependent manner. The contractile stress of the iPSC-CMs increased with a higher strain magnitude and plateaued at 15% cyclic strain. Increasing monolayer contractility corresponded to an enhanced cell and sarcomeric alignment, improved sarcomeric structure, and a higher expression of β-myosin heavy chain (MYH7), illustrating how optimal mechanical strain conditions facilitate a consistent maturation of the cardiomyocyte phenotype and proteome.

2. Material and methods

2.1. Fabrication of microdevice arrays

Each microdevice array consists of three separately contained assay constructs on a single glass slide, each of these possessing a suspended PDMS membrane covered by a softer PDMS film embedded with fluorescent nanobeads. Detailed fabrication steps are provided in Supplementary Fig. S1. In brief, PDMS was mixed at a 10:1 ratio with curing agent, poured into an aluminum mold, and baked at 80 °C for 4 h. The baked PDMS structure was peeled off, treated by plasma and bonded to the glass slide to form the suspended membrane. To measure the contractile stress of iPSC-CM monolayers cultured on the device, softer PDMS (60:1 as the ratio of base polymer and curing agent) was mixed with fluorescent beads (0.2 μm in diameter; fluorescence: λ_{ex} ~575 nm, λ_{em} ~610 nm; Sigma) and spin-coated at 2000 rpm for 1 min to form a thin film on the top surface of the suspended membrane (see fluorescence image in Fig. 1A). The microdevice array was then oven-baked overnight at 80 °C. Custom-made glass cylinders (8 mm in diameter and 10 mm in height for the glass wall) were bonded to each individual device to form independent cell culture chambers (Fig. S1).

2.2. Device calibration and analysis

For device calibration, a pressure control system (Flow EZ, Fluigent) was used to provide pneumatic pressure into the underlying microchannels through a plastic tubing to bulge the suspended membranes. Supplementary Video S1 shows the side-view of a suspended membrane under different actuation pressures. The deflection magnitude Δh at the top center of the suspended membrane, including the softer PDMS film, was analyzed in ImageJ (1.8, National institutes of Health, USA). Finite element analysis (FEA) of membrane strain profiles and vertical displacements was conducted in COMSOL Multiphysics. The device dimensions, material properties of the suspended membrane, and the applied pneumatic pressure were used as input for FEA. PDMS was modeled as an isotropic elastic material with a Poisson's ratio of 0.49. Atomic force microscopy (AFM) indentation was performed (Fig. S2) to measure the elastic modulus value of both the suspended PDMS membrane (1036.1 ± 5.54 kPa, n = 3 independent measurements) and the softer top PDMS film (31.7 ± 1.52 kPa, n = 3 independent measurements). Loop function in COMSOL was employed to calculate Δh and the strain profile under different pneumatic pressures.

Supplementary data related to this article can be found at https://doi.org/10.1016/j.bios.2020.112875.

2.3. iPSC-CMs culture

A monolayer of iPSC-CMs (iCell2®, Cellular Dynamics International) was independently cultured on each of the three membrane constructs per microdevice array, according to the previously outlined protocol (Dou et al., 2020; Wang et al., 2020). Prior to culturing, all devices were sterilized and activated by ultraviolet exposure for 30 min. Device membranes were then coated with an ECM protein mixture, including fibronectin (10 μg/mL) (356008, Corning), gelatin (0.1% w/v) (G1890, Sigma) and laminin (10 μg/mL) (CC095, Sigma), and incubated at 37 °C overnight. Cardiomyocytes were thawed in plating medium (Cellular Dynamics International) and plated at a density of 1.5×10^5 cells/cm^2. Four hours post-plating, the plating medium was replaced with maintenance medium (Cellular Dynamics International). Cell monolayers were cultured in an incubator (37 °C, 5% CO_2) for 10 days. Culture medium (200 μL in volume) was replaced every second day.

2.4. Quantification of cell contractility

The contractile stress of each iPSC-CM monolayer was quantified using traction force microscopy (TFM) (Ribeiro et al., 2017; Tseng et al.,

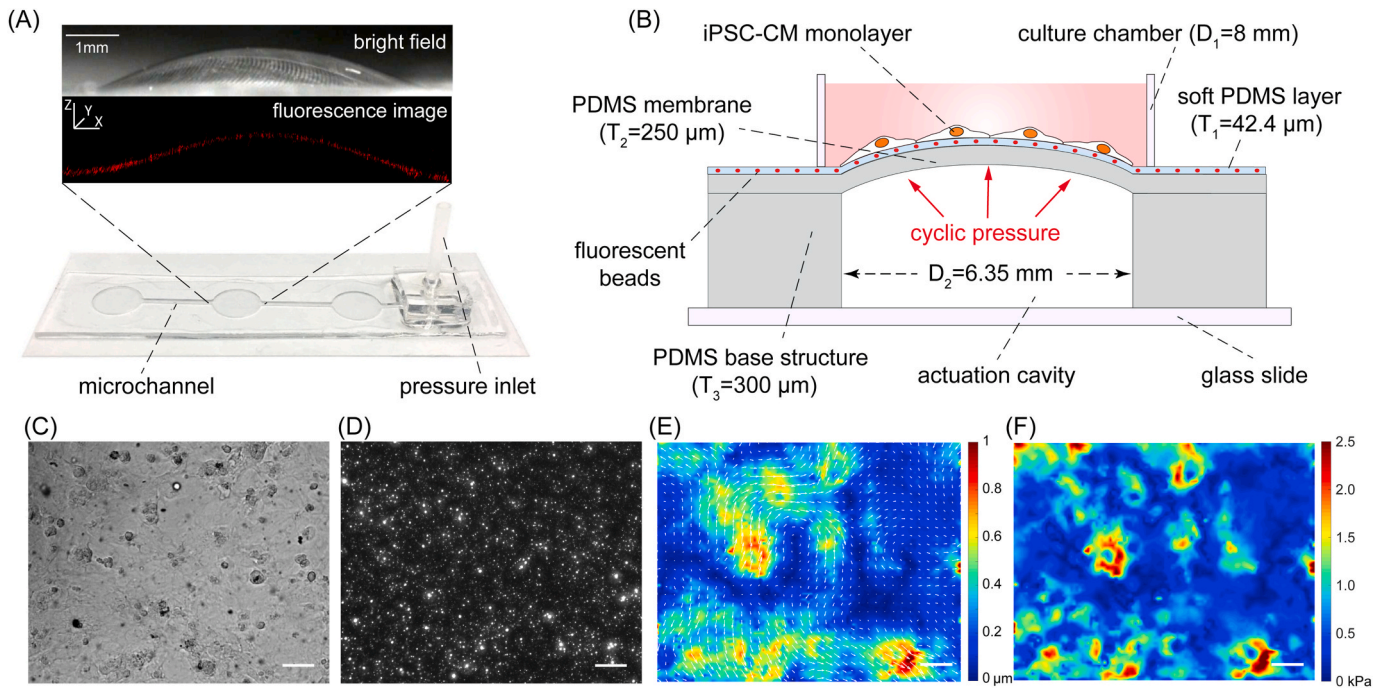

Fig. 1. Microdevice platform for simultaneous mechanical stimulation and contractility measurement of iPSC-CM monolayer. Representative image (A) and schematic diagram (B) of a microdevice array including a pressure inlet, PDMS base structure, microchannel, suspended PDMS membrane, and soft PDMS layer embedded with fluorescent beads. The inset of (A) shows the bright field and fluorescence image (layer with fluorescent beads) of the actuated membrane. Scale bar: 1 mm. (C) iPSC-CMs form a monolayer on the top surface of the suspended membrane. Cells are stimulated by cyclic strain under defined magnitudes. (D) Fluorescence image of the soft PDMS layer embedded with fluorescent beads (0.2 μm in diameter). (E) Representative displacement field of fluorescent beads calculated at the maximal contraction state. Cell contraction induces the movement of embedded fluorescent beads. (F) The corresponding contractile stress field of the same iPSC-CM monolayer at the maximal contraction state. Contractile stress produced by iPSC-CM monolayers are calculated by traction force microscopy (TFM) throughout ten days of cell culture. Scale bar: 50 μm.

2012). Brightfield images of cell contraction and the corresponding movement of fluorescent beads were captured by an Axio Observer microscope (Zeiss, Germany) under controlled temperature and CO_2 concentration (37 °C, 5% CO_2). Videos were recorded at the center of each membrane, under a 20X objective, at 30 frames per second. For each contraction cycle, fluorescent images at the maximal contraction state were compared with the corresponding images at the maximal relaxation state to calculate the displacement field, using standard image cross-correlation techniques. Based on the displacement field and the measured substrate elastic modulus, contraction magnitudes and distributions of iPSC-CMs in the monolayer were calculated using Fourier-Transform Traction Cytometry (FTTC), averaged throughout the imaged area (see Supplementary Materials for details).

2.5. Immunofluorescence staining and sarcomere orientation measurement

Cardiomyocytes were stained for α-actinin and β-myosin heavy chain (MYH7) to evaluate the effect of mechanical stimulation on cell maturation. After day ten, cells were fixed with 4% paraformaldehyde and permeabilized with 0.1% Triton X-100. Following permeabilization, the cells were blocked with antibody diluent solution (5% goat serum in TBST) for 1 h, and then co-stained with mouse anti-α-actinin (1:500, ab9465, Abcam), and rabbit anti-MYH7 (1:100, HPA001239, Sigma) diluted in TBST, overnight at 4 °C. Cells were washed three times with TBST wash buffer (0.01% Triton X-100 in TBS) and incubated with Alexa Fluor® 594-anti-rabbit and Alexa Fluor® 594-anti-mouse secondary antibodies (Cell Signaling Technology) at 1:1000 dilution in TBST with Hoechst 33342 solution (Thermo Scientific) for 1 h at room temperature. The cells were washed again. Fluorescence images were captured on a Quorum spinning disk confocal microscope and analyzed in ImageJ. Sarcomere orientation was measured as the relative angle between the sarcomere elongation direction and the radial direction at the specific location of the suspended membrane. A degree of 0° denotes that sarcomere aligns along the radial direction and 90° denotes that sarcomere aligns along the circumferential direction. Data were analyzed by image processing using OrientationJ plugin for ImageJ (Paparelli et al., 2016).

2.6. Statistical analysis

OriginPro-2018 software was used for statistical analysis. For differential analysis, Student's t-test was performed for comparison between two groups, and one-way ANOVA with a Tukey post hoc test was used to analyze significance between multiple groups. The statistical significance was accepted at the *p-value* < 0.05 ($^{*}p < 0.05$ and $^{**}p < 0.01$ versus control; $\#p < 0.05$ and $\#\#p < 0.01$ for comparisons between groups under mechanical stimulation, ns = not significant). Data were expressed as mean values with the standard error of the mean (mean ± SEM).

3. Results

3.1. Characterization of mechanical strain microdevice array

The described microdevice arrays were adapted from our previous platforms (Liu et al., 2016; Wang et al., 2018) to provide cyclic mechanical stimulation to iPSC-CMs and quantify the development of cell contractility under different strain magnitudes. Each array contained three suspended circular membranes, each 6.35 mm in diameter and 250 μm in thickness, spaced 15 mm center to center (Fig. 1A&B). The softer PDMS film had a thickness of 42.4 ± 0.58 μm as measured using confocal Z-stack images (Fig. S2A), with a Young's modulus of 31.7 ± 1.52 kPa quantified by AFM indentation (n = 3 independent

measurements) (Fig. S2B&C). iPSC-CMs formed a spontaneously beating monolayer on the top membrane surface (Fig. 1C). Cell contraction induced periodic displacements of fluorescent beads embedded in the membrane (Fig. 1D&E), which were used for contractile stress quantification (Fig. 1F; Supplementary Video S2).

Supplementary data related to this article can be found at https://doi.org/10.1016/j.bios.2020.112875.

We calibrated the relationship between membrane deflection magnitude, strain magnitude and applied actuation pressure. Different pneumatic pressures were applied to bulge the device membrane, and the corresponding vertical displacements (Δh) at the center of the membrane were experimentally measured (Fig. 2A&B). In addition, FEA was used to calculate Δh and the equivalent strain profile on the top membrane surface under different actuation pressures. As shown in Fig. 2B, FEA simulation results matched the experimental data (repeated devices, n = 3) with an average error of 2.9%.

The relationship between maximal equivalent strain and applied pressure was calculated by FEA (Fig. 2C), which was used to determine the required pneumatic pressure (1.54 kPa, 4.10 kPa, 8.46 kPa, and 14.79 kPa) to produce the desired strain magnitudes (5%, 10%, 15%, and 20%). The overall experimental setup is shown in Fig. S3 iPSC-CMs adhered to the membrane surface were mechanically stimulated by the device membrane. Fig. S4 shows the equivalent strain distribution on the top membrane surface under each loading condition. The equivalent strain magnitude remains relatively constant in the center area of the membrane and decreases when approaching the membrane boundary (Fig. 2D). To minimize the influence of strain variation across the membrane surface, a region of interest (ROI) was set as the circular area within 1 mm radial distance from the membrane center, and only cells in the ROI were analyzed. The defined ROI minimized the strain variation to be less than 0.8% for all the loading conditions. In addition, a fatigue test was performed to evaluate the potential structural degradation of the device membrane during cyclic bulging. After 10 days (8.6×10^5 cycles) of dynamic stimulation under 15 kPa, neither the Young's modulus nor the maximum displacement (Δh) of the membrane showed a significant change (Fig. 2E), which validated the stability of the devices for mechanical stimulation over a prolonged period.

3.2. Mechanical stimulation increases iPSC-CM contractility

After seeding, iPSC-CMs were cultured statically for 48 h to allow for membrane adherence and the development of a spontaneously beating monolayer (coordinated monolayer contraction). Mechanical stimulation of each cell monolayer was performed by applying cyclic strain (1 Hz) at different strain magnitudes (5%, 10%, 15% and 20%) from day 2 to day 10. For each strain magnitude, three cell monolayers were stimulated as repeated experiments. Dynamic mechanical stimulations were paused for 30 mins at the end of each culture day for the measurement of monolayer contractions in a live imaging system (Zeiss, Germany). The contractile stress of each iPSC-CM monolayer was quantified by measuring the displacements of the fluorescent beads induced by cell contraction (Supplementary Video S2).

The observed changes to each monolayer's contractile stress from day 2 to day 10 was quantified, as shown in Fig. 3A. For all loading

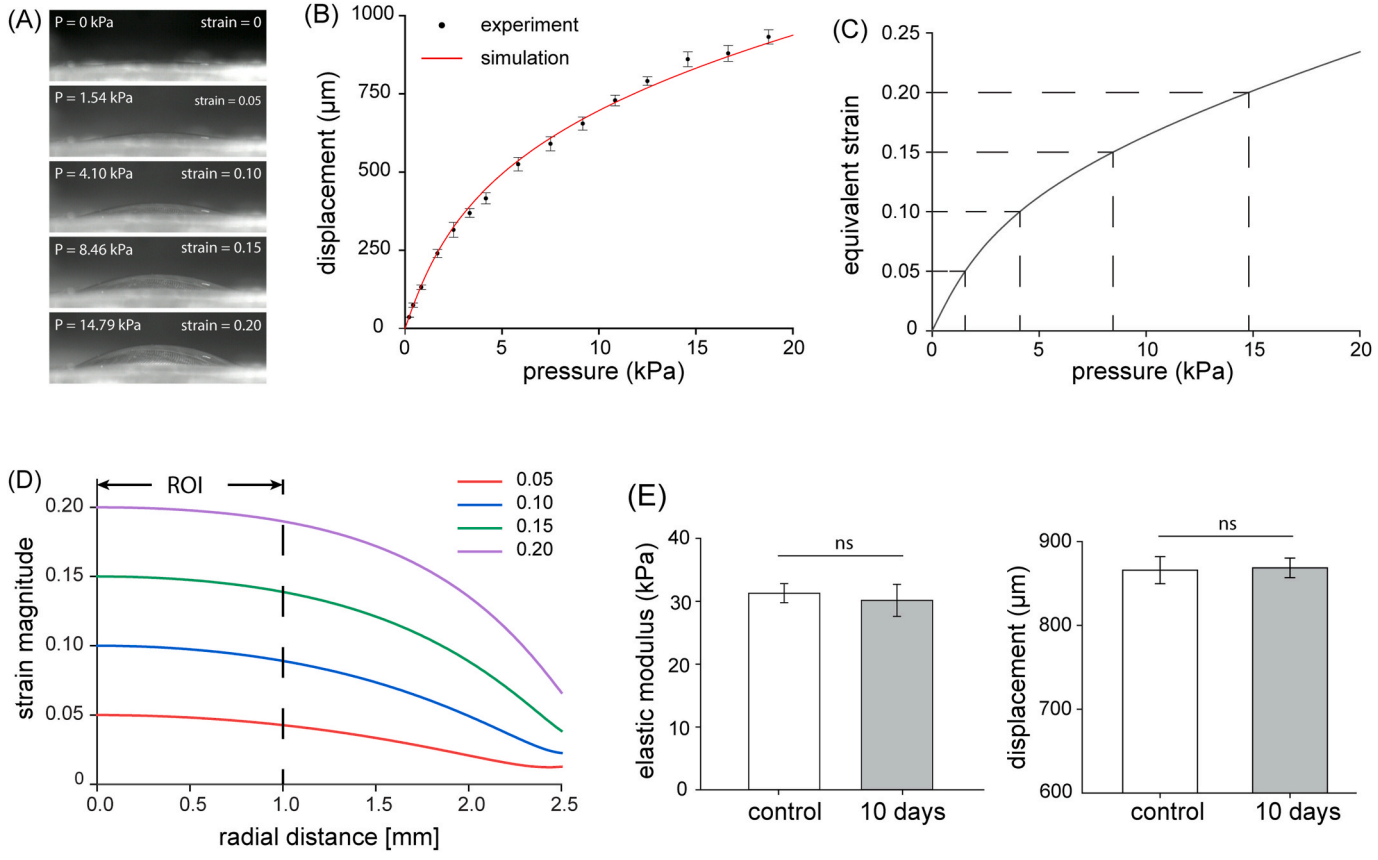

Fig. 2. Device characterization and calibration. (A) Bright-field images showed the deflection of suspended PDMS membrane under defined actuation pressures. (B) Experimental and finite element analysis (FEA) results showed the relationship between membrane vertical displacement and applied pressure, (repeated devices, n = 3). (C) FEA was used to determine the required actuation pressure for each strain magnitude. (D) Equivalent strain profiles along the radial axis under defined loading conditions. Area within 1 mm radial distance is selected as the region of interest (ROI) to minimize strain variations across the membrane surface (less than 0.8%), while containing sufficient cell population for imaging and analysis. (E) Fatigue testing was performed by applying cyclic pressure (15 kPa, 1 Hz) for 10 days. Neither the stiffness of the soft PDMS layer nor the maximum membrane displacement (Δh) showed a significant change before and after fatigue testing (repeated membranes, n = 3).

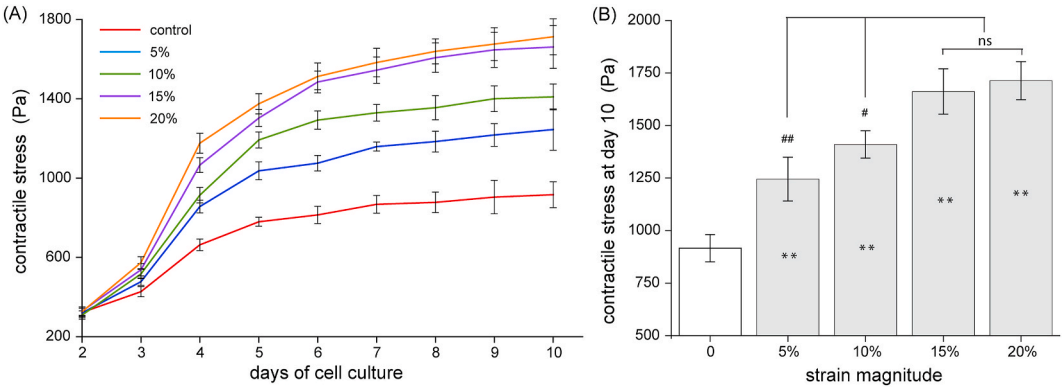

Fig. 3. Enhancement of iPSC-CM contractility with mechanical stimulation. (A) Representative curves of the development of contractile stress during 10 days of cell culturing. Cell monolayers were stimulated under defined strain magnitudes (control, 5%, 10%, 15% and 20%) from day 2 to day 10. (B) Quantification of the improvement in contractile stress at each stimulation condition after 10 days of cell culture. Repeated monolayers of each condition, n = 3. *p < 0.05 and **p < 0.01 versus control; # p < 0.05 and ## p < 0.01 for comparisons between groups under mechanical stimulation.

conditions (0%, 5%, 10%, 15% and 20% mechanical strain), a time-dependent increase in the contractility of iPSC-CM monolayers was seen. Cells initiated beating on day 2 and displayed synchronous contraction thereafter. When compared to the control group (i.e., 0% strain), mechanical stimulation improved the contractility of the iPSC-CMs after day 3 (Fig. 3A). For each loading condition, cell contractility increased nonlinearly during the 10-day period. For instance, for the group loaded with 10% strain, contractile stress exhibited a substantial increase from day 2 to day 6 (308.76 ± 20.47 Pa to 1292.85 ± 46.3 Pa, n = 3 monolayers), and then slowly increased from day 6 to day 10 (1292.85 ± 46.3 Pa to 1409.85 ± 64.87 Pa, n = 3 monolayers).

Fig. 3B summarizes the contractile stress of all the iPSC-CM monolayers at day 10, for each strain magnitude of loading. Compared with the control group (0% strain), contractile stress significantly increased from 916.12 ± 65.11 Pa to 1244.95 ± 104.41 Pa for 5% strain, to 1409.85 ± 64.87 Pa for 10% strain, and to 1661.68 ± 108.02 Pa for 15% strain. The contractile stress plateaued at the 15% strain magnitude, and no significant difference was observed between the 15%-strain group and the 20%-strain group (1713.48 ± 91.03 Pa, p = 0.94, n = 3 monolayers for each loading condition). Even up to 20% strain, no downward trend was observed.

3.3. Sarcomere and MYH7 expression enhancement under mechanical stimulation

To investigate whether the observed increase in cardiomyocyte contraction correlated to an increase in cell maturation, we probed for two key cardiomyocyte proteins (α-actinin and MYH7) by immunofluorescence at the end of the 10-day culture period. α-actinin was used to quantify sarcomeric structure and alignment, where MYH7 (β-myosin heavy chain) was used to assess iPSC-CM maturity as the isoform predominantly expressed in adult human hearts (Zhu et al., 2014).

We found that mechanical stimulation applied to iPSC-CMs by the bulged membrane promoted overall intercellular alignment, as determined by α-actinin staining. Confocal images of iPSC-CMs stimulated with different strain magnitudes were captured at a 1 mm radial distance away from the membrane center for cell alignment analysis. Sarcomere orientation (Fig. 4A) depends on the strain magnitude and exhibited gradual change from random directions to the direction perpendicular to the radial direction (circumferential direction) with the increase of strain magnitudes. It suggested that a larger cyclic strain magnitude has stronger effects on inducing cardiomyocyte sarcomere alignment. The immunohistochemistry images (Fig. 4B and C) in both control group and 20% strain group clearly indicated that cells reoriented along the circumference of the membrane bulge under mechanical stimulation. Comparing with the sarcomere orientations at the membrane center (Fig. S5), the "strain-avoidance" cell alignment along the circumferential direction was supposed to be determined by the magnitude difference of applied strain in radial and circumferential directions (Fig. S6) at the targeted imaging positions.

Fig. 5A shows that mechanical stimulation shifted sarcomere structures from random patterns (control group) to striate and parallel patterns (mechanically stimulated group). Sarcomere length, summarized in Fig. 5B, was determined by measuring the distance between neighboring α-actinin bands. Relative to the control group, the cardiomyocyte populations under cyclic stain displayed an increase in the sarcomere length (control: 1.746 ± 0.196 μm; 5% strain: 1.806 ± 0.030 μm; 10% strain: 1.890 ± 0.027 μm; 15% strain: 1.908 ± 0.033 μm; 20% strain: 1.911 ± 0.030 μm, n = 35 sarcomeres for each condition). Compared to the loading strain of 10%, no significant improvement of sarcomere length was observed with a further increase of strain magnitude. Elongation of sarcomere length induced by mechanical stimulation follows the Frank-Starling Law (Delicce et al., 2019), enabling cells to produce a larger sliding distance between the actin and myosin filaments during contraction, and hence increase cell contractility.

We also evaluated the expression level of MYH7 by normalizing the fluorescence intensity to that of the control group, as shown in Fig. 5A&C. In contrast to the plateaued increase in contractility and sarcomere length, MYH7 expression was upregulated in a strain-dependent manner at all tested strain magnitudes. We attempted to further increase the loading magnitude to 25% and evaluate whether MYH7 expression increased further. However, the iPSC-CM monolayers partially detached from the device membrane and formed separated clusters under these high mechanical strain conditions (Fig. S7).

4. Discussion

The generation of functional human cardiomyocytes through induced pluripotent stem cells allows for more accurate disease modeling to study pathobiology and facilitate therapeutic discovery. However, the immature (fetal-like) phenotype of these cells has limited their translational potential. Cyclic mechanical loading experienced by developing hearts is widely recognized to be indispensable for cardiomyocyte maturation and contractility (Guo and Pu, 2020). Accordingly, several platforms have attempted to integrate different forms of mechanical or electromechanical stimulation to study mechanotransduction in iPSC-CMs and promote cell maturation *in vitro* (Carson et al., 2016; Marsano et al., 2015; Nunes et al., 2013; Tiburcy et al., 2017). In the present study, we developed a microdevice platform to apply cyclic strain to a monolayer of iPSC-CMs to more closely emulate the developmental environment and to allow for tunable changes to cell maturation conditions. Our results quantitatively illustrate how

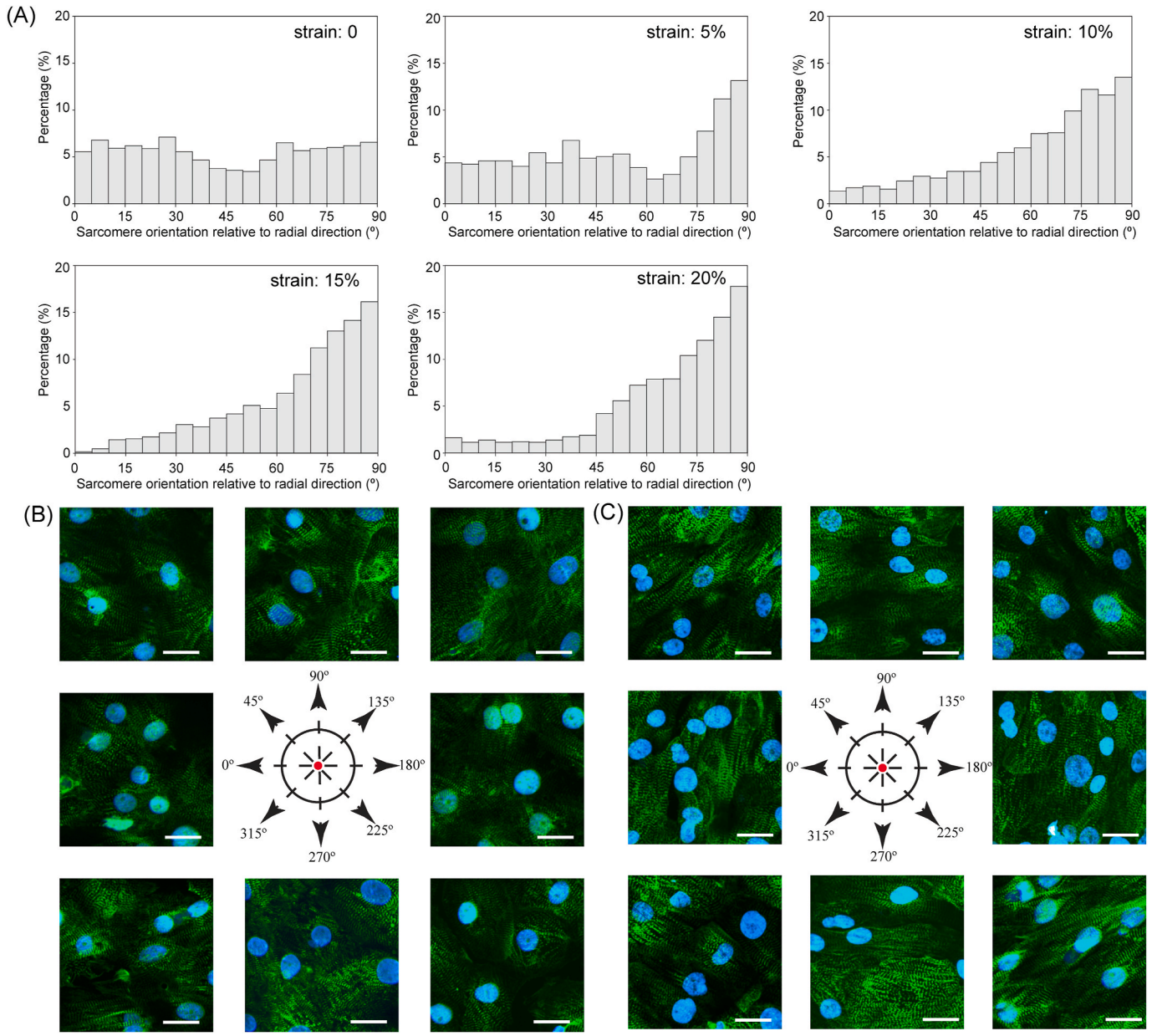

Fig. 4. Mechanical stimulation enhances the alignment of iPSC-CMs. (A) Distribution of sarcomere orientations under different mechanical loading conditions (control, 5%, 10%, 15% and 20%). Sarcomere orientations relative to the membrane radial direction were measured at areas with ~1 mm radial distance from the membrane center. (B and C) Confocal images of iPSC-CMs under (B) 0 strain and (C) 20% cyclic strain conditions and captured at areas with ~1 mm radial distance from the membrane center (red dot). Cells illustrate better intra- and inter-cellular alignment of sarcomeres (α-actinin, green). Cyclic strain induces circumferential cell alignment on the actuated membranes. Scale bar: 25 μm. (For interpretation of the references to colour in this figure legend, the reader is referred to the Web version of this article.)

different mechanical strain magnitudes regulate the contractile stress and maturity of iPSC-CMs, in terms of cell alignment, sarcomere length, and MYH7 expression.

Compared to mechanically active bioreactors (Dhein et al., 2014; Shao et al., 2013), microdevice platforms for mechanical stimulation of cultured cells have lower complexity in setup and increased throughput (Marsano et al., 2015; Parsa et al., 2017). However, due to the difficulty of integrating on-chip sensing components, most existing microdevice platforms only allow end-point analyses of cell/tissue functions. Our microdevice arrays are capable of dynamic mechanical stimulation, *in situ* contractility measurement, and on-chip imaging for immunostaining analysis. The strain magnitude on the suspended membrane was accurately controlled by varying the actuation pressure. Although a heterogenous strain profile exists on the membrane surface, spatial heterogeneity was readily mitigated by regional image analysis (Fig. 2D). The Young's modulus of the top soft PDMS layer (31.7 kPa) is comparable with healthy adult myocardium (22–50 kPa) (Bhana et al., 2010). Compared with traditional rigid substrates, cardiomyocytes cultured on surfaces with tissue-like stiffness have been reported to exhibit improved morphology (e.g., sarcomere alignment) and functional properties (e.g., calcium handling and contractility) (Jacot et al., 2008). UV irradiation followed by immediate protein coating (Jastrzebska et al., 2018) was performed to modify the hydrophobic property of the PDMS membrane for cell adhesion. Our results showed that the iPSC-CMs adhered well and formed a spontaneously beating monolayer in both the control group and those mechanically stimulated with up to 20% strain. At 25% strain, we observed cell detachment and the formation of cell clusters. To further improve cell adhesion to sustain

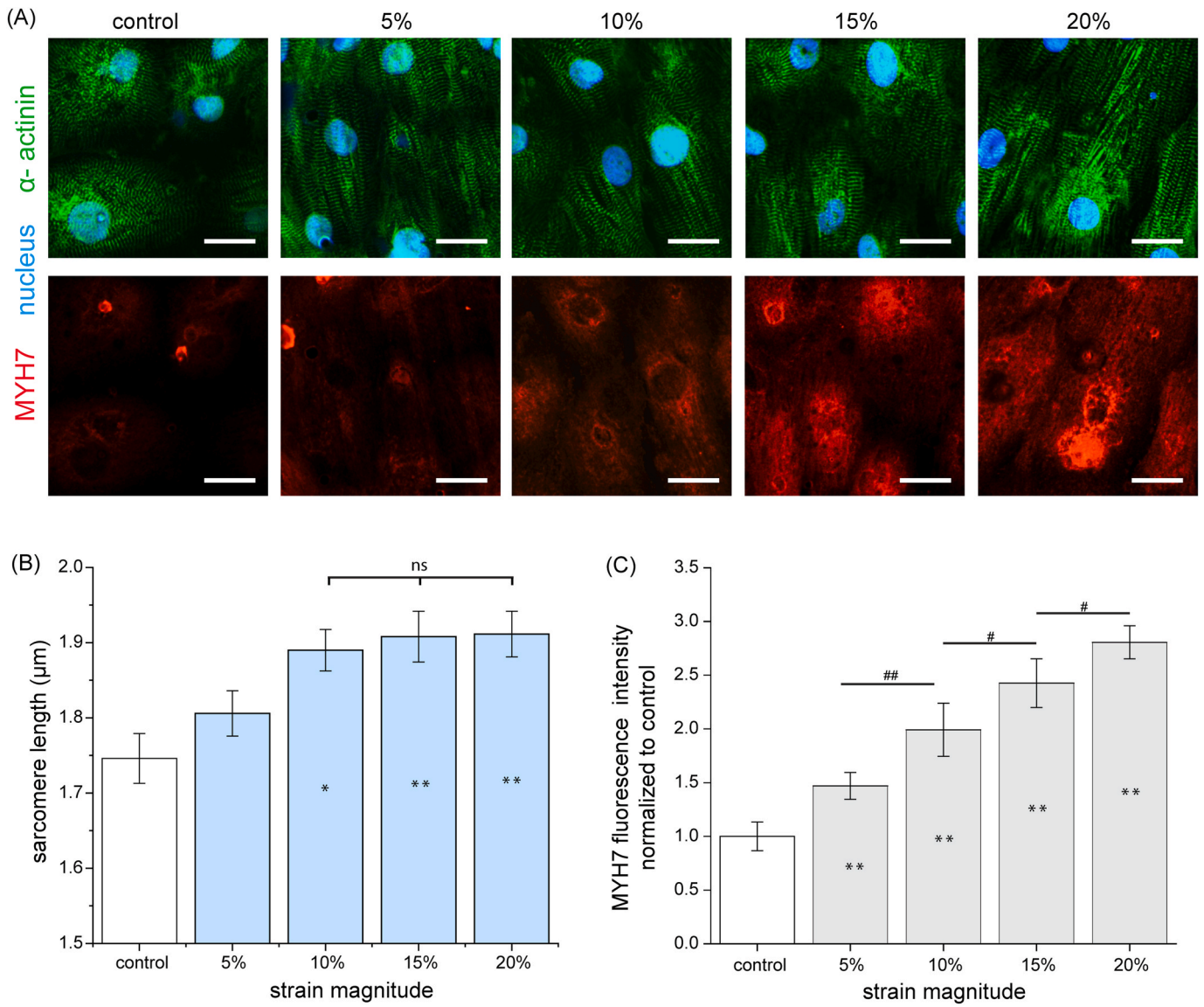

Fig. 5. Changes of contraction-related biomarkers (sarcomere length and MYH7 expression) with the increase of mechanical loading. (A) Representative confocal images of iPSC-CM monolayers under defined strain conditions (day 10). Cells are stained with α-actinin (green), myosin heavy chain-beta (MYH7, red) and nuclei (cyan). (B) Sarcomere length and (C) protein expression of MYH7 were quantified from the immunohistochemistry images. Sarcomere length was measured as the distance between successive α-actinin striations. Measured sarcomeres n = 35 for each condition. The expression levels of MYH7 was calculated by normalizing the fluorescence intensity to the control group. Repeated monolayers n = 3, *$p < 0.05$ and **$p < 0.01$ versus control; $^{\#}p < 0.05$ and $^{\#\#}p < 0.01$ for comparisons between groups under mechanical stimulation. Scale bar: 25 μm. (For interpretation of the references to colour in this figure legend, the reader is referred to the Web version of this article.)

higher mechanical strain magnitudes, potential solutions include progressively increasing stimulation intensity over time, optimizing the membrane coating matrix, and testing other surface modification methods (Beal et al., 2012). However, it may also be that physical cell stretching was maximized at 20%, and de-adherence at further strains was related to the loss of cell:cell junctions. Fatigue testing verified there was no significant variation of membrane stiffness and deflection magnitude throughout the experiment period (Fig. 2E), indicating the operational stability of the microdevices for at least ten days.

Contraction of cardiomyocytes occurs through the conversion of electrical signals to a mechanical response, in a process termed "excitation-contraction coupling" (Bers, 2002). The propagation of the action potential through cell membranes and gap junctions initiates membrane depolarization and triggers the shortening of sarcomeres through crossbridge cycling between actin and myosin filaments. We performed *in situ* monitoring of the dynamic changes to iPSC-CM contractility under different strain magnitudes, quantified over a 10-day culture period. For each loading condition, a time-dependent increase of contractile stress was observed; with rapid increase from day 3 to day 6, followed by moderate increase after day 6 (Fig. 3A). At the time of plating, iPSC-CMs exhibited low cell area, sparse sarcomeres, and minimal intercellular contact. From day 2 to day 6, rapid cell spreading occurred, corresponding to increased cell area, sarcomere development and cell-cell contact. Intercellular contact between adjacent cardiomyocytes facilitated electrical communication, as evidenced by synchronous cell beating and increased contractility. Following day 6, few gross morphological changes were observed for the cells. Cell contractility was further improved by performing mechanical loading through membrane bulging, up to a strain magnitude of 15% (Fig. 3B). Similarly, sarcomere length increased and plateaued at the strain magnitude of 15% (Fig. 5B); however, the expression of MYH7 continued to increase to the highest strain magnitude tested (20%) (Fig. 5C). A mature

sarcomere comprises multiple structural components, including thin filaments (actin), thick filaments (β-myosin heavy chain, myosin binding protein C), titin filaments (titin), Z-disks (α-actinin), and M-lines (myomesin) (Guo and Pu, 2020). We speculate that certain sarcomeric components may respond differently to an increasing magnitude of mechanical stimulation, as multiple mechanotransduction pathways are known to influence cardiomyocyte protein expression, regulation and function (i.e., integrin-mediated force sensing through focal adhesions, transcription regulation through LINC/laminin proteins, among others (Schumacher et al., 2020; Stewart et al., 2019)). Ultrastructural organization of sarcomeres, in terms of length and alignment, could be rapidly modified under lower mechanical loading conditions, while the expression and synthesis of sarcomeric protein isoforms (e.g., MYH7) may require longer durations of strain and/or higher strain magnitudes.

Mechanical strain has been reported to cause reorientation of different cell types along the direction that is perpendicular to the principle strain *in vitro* (Kamble et al., 2018; Qi et al., 2015; Salameh et al., 2010). For cardiomyocytes, the "strain-avoidance" alignment behavior is regulated through mechanotransduction to help cells minimize the perturbation of applied strain on cell contraction and cell adhesion (Mauretti et al., 2016; Salameh et al., 2010). Three orthogonal strain components (radial, circumferential, and longitudinal) exist in the human heart *in vivo*, and the global mean systolic strain of human heart's left ventricular wall in the radial direction (38.8 ± 7.3%) is approximately two times larger than that in the circumferential direction (18.5 ± 2.0%) (Liu et al., 2017). Meanwhile, the muscle fibers in the heart generally show circumferential alignment in myocardium and encircle the heart chambers with helical angles (Doste et al., 2019; Rijcken et al., 1999). The "strain-avoidance" response of cardiomyocyte alignment on our bulging membrane microdevice likely resulted from the magnitude difference of applied strains in the radial and circumferential directions.

At 15% strain magnitude, our microdevice platform improved iPSC-CMs contractility by 87% relative to the control group at day 10, and the achieved contractile stress of iPSC-CMs is higher than the highest value previously reported via mechanical stimulation (1.71 kPa vs. 1.05 kPa) (Ruan et al., 2015). To further enhance cardiomyocyte maturation and contractility, combinatorial stimuli will likely need to be tested, including electrical stimulation (Nunes et al., 2013), substrate topography (Carson et al., 2016), delivery of biochemical factors (including those from other cell types like fibroblasts) (Laflamme et al., 2007), and regulation of gene expression (Takahashi et al., 2007). Our next steps are to incorporate these types of stimuli into our microdevice arrays to investigate their effects on iPSC-CMs and further improve cell maturation *in vitro*.

In addition to cell maturation, our device provides an intriguing way to model the mechanical stress (and cellular response) to a dilating, failing ventricle. In many forms of heart failure, the cardiac ventricles undergo a progressive dilation as a result of pressure overload either pressure from flow limitation (stenosis) or increased pumping volume (valve insufficiency causing a back-flow of blood (Goh et al., 2017; Vonk Noordegraaf et al., 2017)). It is recognized that the failing ventricle responds differently to corrective pharmacology (e.g., inotropes), compared to a healthy heart (Ahmad et al., 2019; Farmakis et al., 2019) The ability to provide a tunable, repetitive stress on the functional cardiomyocyte monolayer offers the possibility of emulating ventricular wall stress, with the subsequent quantification of contractility after the administration of a potential therapeutic. This capacity would be specifically useful in modeling cardiac diseases with a maladaptive response to mechanical stress (Brayson and Shanahan, 2017).

5. Conclusion

Mechanical cues play a key role in regulating cellular functions and maintaining homeostasis. The work presented here focused on quantifying the effect of different mechanical strain magnitudes on the contractility and maturation of iPSC-CMs. We developed a microdevice platform to mechanically stimulate monolayers of iPSC-CMs with strain magnitudes ranging from 5% to 20%. *In situ* measurement of contractility iPSC-CMs was realized by embedding fluorescent nanobeads in the device membrane and performing traction force microscopy. Our experimental results show that cell contractility was enhanced in a strain magnitude-dependent manner and plateaued at 15% strain. Improvement in overall cell alignment, sarcomeric structure, and MYH7 expression were concurrent with the increase in iPSC-CM contractility. Our results highlight the importance of accounting for mechanical strain magnitude when creating *in vitro* cardiac models to ensure that the cellular phenotype represents an adult cardiomyocyte, improving the applicability and potential clinical translation of findings.

CRediT authorship contribution statement

Wenkun Dou: Conceptualization, Investigation, Methodology, Data curation, Writing - original draft. **Li Wang:** Conceptualization, Methodology, Data curation. **Manpreet Malhi:** Methodology, Investigation, Data curation, Writing - original draft. **Haijiao Liu:** Investigation, Data curation. **Qili Zhao:** Methodology, Validation. **Julia Plakhotnik:** Investigation, Visualization. **Zhensong Xu:** Methodology, Visualization. **Zongjie Huang:** Methodology, Visualization. **Craig A. Simmons:** Resources, Validation, Supervision, Writing - review & editing. **Jason T. Maynes:** Conceptualization, Resources, Validation, Supervision, Writing - review & editing. **Yu Sun:** Conceptualization, Resources, Validation, Supervision, Writing - review & editing, Project administration.

Declaration of competing interest

The authors declare that they have no known competing financial interests or personal relationships that could have appeared to influence the work reported in this paper.

Acknowledgements

The authors acknowledge the financial support from the Canadian Institutes of Health Research (CIHR) and the Natural Sciences and Engineering Research Council of Canada (NSERC) through a Collaborative Health Research Projects (CHRP) grant. Y.S. also acknowledges the financial support from the Canada Research Chairs Program and the Ontario Research Fund – Research Excellence Program. W.K.D. acknowledges a fellowship from the Ted Rogers Centre for Heart Research Education Fund. J.T.M. would like to thank his clinical colleagues for protected time, and the Wasser Family and the SickKids Foundation for Chair funds.

Appendix A. Supplementary data

Supplementary data to this article can be found online at https://doi.org/10.1016/j.bios.2020.112875.

References

Ahmad, T., Miller, P.E., McCullough, M., Desai, N.R., Riello, R., Psotka, M., Böhm, M., Allen, L.A., Teerlink, J.R., Rosano, G.M.C., Lindenfeld, J., 2019. Eur. J. Heart Fail. 21, 1064–1078.

Banerjee, I., Carrion, K., Serrano, R., Dyo, J., Sasik, R., Lund, S., Willems, E., Aceves, S., Meili, R., Mercola, M., Chen, J., Zambon, A., Hardiman, G., Doherty, T.A., Lange, S., del Álamo, J.C., Nigam, V., 2015. J. Mol. Cell. Cardiol. 79, 133–144.

Beal, J.H.L., Bubendorfer, A., Kemmitt, T., Hoek, I., Mike Arnold, W., 2012. Biomicrofluidics 6, 1–11.

Benjamin, E.J., Muntner, P., Alonso, A., Bittencourt, M.S., Callaway, C.W., Carson, A.P., Chamberlain, A.M., Chang, A.R., Cheng, S., Das, S.R., 2019. Circulation others.

Bers, D.M., 2002. Nature 415, 198–205.

Bhana, B., Iyer, R.K., Chen, W.L.K., Zhao, R., Sider, K.L., Likhitpanichkul, M., Simmons, C.A., Radisic, M., 2010. Biotechnol. Bioeng. 105, 1148–1160.

Brayson, D., Shanahan, C.M., 2017. Nucleus 8, 17–33.

Carson, D., Hnilova, M., Yang, X., Nemeth, C.L., Tsui, J.H., Smith, A.S.T., Jiao, A., Regnier, M., Murry, C.E., Tamerler, C., Kim, D.H., 2016. ACS Appl. Mater. Interfaces 8, 21923–21932.
Delicce, A.V., Basit, H., Makaryus, A.N., 2019. Physiology, Frank Starling Law. StatPearls Publishing, Treasure Island (FL).
Dhein, S., Schreiber, A., Steinbach, S., Apel, D., Salameh, A., Schlegel, F., Kostelka, M., Dohmen, P.M., Mohr, F.W., 2014. Prog. Biophys. Mol. Biol. 115, 93–102.
Doste, R., Soto-Iglesias, D., Bernardino, G., Alcaine, A., Sebastian, R., Giffard-Roisin, S., Sermesant, M., Berruezo, A., Sanchez-Quintana, D., Camara, O., 2019. Int. J. Numer. Method. Biomed. Eng. 35, 1–17.
Dou, W., Zhao, Q., Malhi, M., Liu, X., Zhang, Z., Wang, L., Masse, S., Nanthakumar, K., Hamilton, R., Maynes, J.T., Sun, Y., 2020. Biosens. Bioelectron. 167, 112468.
Farmakis, D., Agostoni, P., Baholli, L., Bautin, A., Comin-Colet, J., Crespo-Leiro, M.G., Fedele, F., Garc\'\ia-Pinilla, J.M., Giannakoulas, G., Grigioni, F., 2019. others. Int. J. Cardiol. 297, 83–90.
Feric, N.T., Radisic, M., 2016. Adv. Drug Deliv. Rev. 96, 110–134.
Goh, V.J., Le, T.T., Bryant, J., Wong, J.I., Su, B., Lee, C.H., Pua, C.J., Sim, C.P.Y., Ang, B., Aw, T.C., Cook, S.A., Chin, C.W.L., 2017. Circ. Cardiovasc. Imag. 10, 1–10.
Guo, Y., Pu, W.T., 2020. Circ. Res. 126, 1086–1106.
Hove, J.R., Köster, R.W., Forouhar, A.S., Acevedo-Bolton, G., Fraser, S.E., Gharib, M., 2003. Nature 421, 172–177.
Jacot, J.G., McCulloch, A.D., Omens, J.H., 2008. Biophys. J. 95, 3479–3487.
Jastrzebska, E., Zuchowska, A., Flis, S., Sokolowska, P., Bulka, M., Dybko, A., Brzozka, Z., 2018. Biomicrofluidics 12, 1–14.
Kamble, H., Vadivelu, R., Barton, M., Shiddiky, M.J.A., Nguyen, N.T., 2018. Lab Chip 18, 765–774.
Laflamme, M.A., Chen, K.Y., Naumova, A.V., Muskheli, V., Fugate, J.A., Dupras, S.K., Reinecke, H., Xu, C., Hassanipour, M., Police, S., O'Sullivan, C., Collins, L., Chen, Y., Minami, E., Gill, E.A., Ueno, S., Yuan, C., Gold, J., Murry, C.E., 2007. Nat. Biotechnol. 25, 1015–1024.
Lindsey, S.E., Butcher, J.T., Yalcin, H.C., 2014. Front. Physiol. 5 (AUG), 1–15.
Liu, H., Usprech, J., Sun, Y., Simmons, C.A., 2016. Acta Biomater. 34, 113–124.
Liu, H., Yang, D., Wan, K., Luo, Y., Sun, J.Y., Zhang, T.J., Li, W.H., Greiser, A., Jolly, M. P., Zhang, Q., Chen, Y.C., 2017. Sci. Rep. 7, 1–9.
Liu, Y.W., Chen, B., Yang, X., Fugate, J.A., Kalucki, F.A., Futakuchi-Tsuchida, A., Couture, L., Vogel, K.W., Astley, C.A., Baldessari, A., Ogle, J., Don, C.W., Steinberg, Z.L., Seslar, S.P., Tuck, S.A., Tsuchida, H., Naumova, A.V., Dupras, S.K., Lyu, M.S., Lee, J., Hailey, D.W., Reinecke, H., Pabon, L., Fryer, B.H., MacLellan, W. R., Thies, R.S., Murry, C.E., 2018. Nat. Biotechnol. 36, 597–605.
Marsano, A., Conficconi, C., Lemme, M., Occhetta, P., Gaudiello, E., Votta, E., Cerino, G., Redaelli, A., Rasponi, M., 2015. Lab Chip 16, 599–610.
Mauretti, A., Bax, N.A.M., Van Marion, M.H., Goumans, M.J., Sahlgren, C., Bouten, C.V. C., 2016. Integr. Biol. (United Kingdom) 8, 991–1001.
Mihic, A., Li, J., Miyagi, Y., Gagliardi, M., Li, S.H., Zu, J., Weisel, R.D., Keller, G., Li, R.K., 2014. Biomaterials 35, 2798–2808.
Miklas, J.W., Nunes, S.S., Sofla, A., Reis, L.A., Pahnke, A., Xiao, Y., Laschinger, C., Radisic, M., 2014. Biofabrication 6.
Nunes, S.S., Miklas, J.W., Liu, J., Aschar-Sobbi, R., Xiao, Y., Zhang, B., Jiang, J., Massé, S., Gagliardi, M., Hsieh, A., Thavandiran, N., Laflamme, M. a, Nanthakumar, K., Gross, G.J., Backx, P.H., Keller, G., Radisic, M., 2013. Nat. Methods 10, 781–787.
Paparelli, L., Corthout, N., Pavie, B., Annaert, W., Munck, S., 2016. Analyzing protein clusters on the plasma membrane: application of spatial statistical analysis methods on super-resolution microscopy images. Advances in Anatomy Embryology and Cell Biology.
Parsa, H., Wang, B.Z., Vunjak-Novakovic, G., 2017. Lab Chip 17, 3264–3271.
Qi, Y., Li, Z., Kong, C.W., Tang, N.L., Huang, Y., Li, R.A., Yao, X., 2015. J. Mol. Cell. Cardiol. 87, 65–73.
Ribeiro, A.J.S., Schwab, O., Mandegar, M.A., Ang, Y.S., Conklin, B.R., Srivastava, D., Pruitt, B.L., 2017. Circ. Res. 120, 1572–1583.
Rijcken, J., Bovenoeerd, P.H.M., Schoofs, A.J.G., Van Campen, D.H., Arts, T., 1999. Ann. Biomed. Eng. 27, 289–297.
Romagnuolo, R., Masoudpour, H., Porta-Sánchez, A., Qiang, B., Barry, J., Laskary, A., Qi, X., Massé, S., Magtibay, K., Kawajiri, H., Wu, J., Valdman Sadikov, T., Rothberg, J., Panchalingam, K.M., Titus, E., Li, R.K., Zandstra, P.W., Wright, G.A., Nanthakumar, K., Ghugre, N.R., Keller, G., Laflamme, M.A., 2019. Stem Cell Rep. 12, 967–981.
Rowe, R.G., Daley, G.Q., 2019. Nat. Rev. Genet. 20.
Ruan, J.L., Tulloch, N.L., Razumova, M.V., Saiget, M., Muskheli, V., Pabon, L., Reinecke, H., Regnier, M., Murry, C.E., 2016. Circulation 134, 1557–1567.
Ruan, J.L., Tulloch, N.L., Saiget, M., Paige, S.L., Razumova, M.V., Regnier, M., Tung, K. C., Keller, G., Pabon, L., Reinecke, H., Murry, C.E., 2015. Stem Cell. 33, 2148–2157.
Salameh, A., Wustmann, A., Karl, S., Blanke, K., Apel, D., Rojas-Gomez, D., Franke, H., Mohr, F.W., Janousek, J., Dhein, S., 2010. Circ. Res. 106, 1592–1602.
Saucerman, J.J., Tan, P.M., Buchholz, K.S., McCulloch, A.D., Omens, J.H., 2019. Nat. Rev. Cardiol. 16, 361–378.
Schumacher, J.A., Wright, Z.A., Owen, M.L., Bredemeier, N.O., Sumanas, S., 2020. Dev. Biol. 465, 46–57.
Shao, Y., Tan, X., Novitski, R., Muqaddam, M., List, P., Williamson, L., Fu, J., Liu, A.P., 2013. Rev. Sci. Instrum. 84.
Stewart, R.M., Rodriguez, E.C., King, M.C., 2019. Mol. Biol. Cell 30, 1664–1675.
Takahashi, K., Tanabe, K., Ohnuki, M., Narita, M., Ichisaka, T., Tomoda, K., Yamanaka, S., 2007. Cell 131, 861–872.
Tiburcy, M., Hudson, J.E., Balfanz, P., Schlick, S., Meyer, T., Liao, M.L.C., Levent, E., Raad, F., Zeidler, S., Wingender, E., Riegler, J., Wang, M., Gold, J.D., Kehat, I., Wettwer, E., Ravens, U., Dierickx, P., Van Laake, L.W., Goumans, M.J., Khadjeh, S., Toischer, K., Hasenfuss, G., Couture, L.A., Unger, A., Linke, W.A., Araki, T., Neel, B., Keller, G., Gepstein, L., Wu, J.C., Zimmermann, W.H., 2017. Circulation 135, 1832–1847.
Tseng, Q., Duchemin-Pelletier, E., Deshiere, A., Balland, M., Guilloud, H., Filhol, O., Theŕy, M., 2012. Proc. Natl. Acad. Sci. U.S.A. 109, 1506–1511.
Vonk Noordegraaf, A., Westerhof, B.E., Westerhof, N., 2017. J. Am. Coll. Cardiol. 69, 236–243.
Wang, L., Dou, W., Malhi, M., Zhu, M., Liu, H., Plakhotnik, J., Xu, Z., Zhao, Q., Chen, J., Chen, S., Hamilton, R., Simmons, C.A., Maynes, J.T., Sun, Y., 2018. ACS Appl. Mater. Interfaces 10, 21173–21183.
Wang, X., Wang, L., Dou, W., Huang, Z., Zhao, Q., Malhi, M., Maynes, J.T., Sun, Y., 2020. Biosens. Bioelectron. 166, 112399.
Zhang, W., Kong, C.W., Tong, M.H., Chooi, W.H., Huang, N., Li, R.A., Chan, B.P., 2017. Acta Biomater. 49, 204–217.
Zhu, R., Blazeski, A., Poon, E., Costa, K.D., Tung, L., Boheler, K.R., 2014. Stem Cell Res. Ther. 5, 117.